

Experimental Investigation of an Active Twist Model Rotor Blade under Centrifugal Loads

Peter Wierach¹, Johannes Riemenschneider¹, Steffen Optiz¹, Frauke Hoffmann²

¹ Institute of Composite Structures and Adaptive Systems, German Aerospace Center (DLR),
Lilienthalplatz 7, 38108 Braunschweig, Germany
e-mail: peter.wierach@dlr.de

² Institute of Flightsystems, German Aerospace Center (DLR),
Lilienthalplatz 7, 38108 Braunschweig, Germany

Key words: active twist, piezo composites, smart structures, centrifugal test

Abstract: Individual Blade Control (IBC) for helicopter rotors promises to be a method to increase flight performance and to reduce vibration and noise. Quite a few concepts to realize IBC Systems have been proposed so far. Some of them have already been tested in wind tunnels or on real helicopters. A drawback of all systems that include discrete mechanical components like hinges, levers or gears is their vulnerability in a helicopter environment with high centrifugal loads and high vibration levels. That's why the idea of using smart materials that are directly embedded in the rotor blade structure is very attractive for this application. Operating as solid state actuators they can generate a twist deformation of the rotor blade without any friction and wear. In the common DLR-ONERA project "Active Twist Blade" (ATB), DLR designed and build a 1:2.5 mach scaled BO105 model rotor blade incorporating state of the art Macro Fiber Composite (MFC) Actuators. The design of the blade was optimized using a finite element code as well as rotor dynamic simulations to predict the benefits with respect to vibrations, noise and performance. Based on these tools a blade was designed that meets all mass and stiffness constraints. The blade has been intensively tested within some bench- and centrifugal tests. The mechanical properties of the blade obtained within the bench tests showed a good correlation between measured and calculated values. The centrifugal test comprised a measurement of the active twist performance at the nominal rotation speed of 1043 RPM at different excitation frequencies from 2/rev up to 6/rev. It was proven, that also under centrifugal loads the predicted twist amplitudes can be achieved.

INTRODUCTION

For helicopters in forward flight very complex flow conditions are apparent. The superposition of the flight speed of the helicopter to the rotational speed of the main rotor leads to asymmetric flow conditions between advancing and retreating side. This asymmetry of the flow conditions in the rotor disk is growing with increasing flight speed. At the advancing side the flow reaches transonic and supercritical velocity regimes resulting in local shock waves which are a major source of noise in high-speed forward flight. In contrast, regions with flow separation respectively stall occur at the retreating side. Since the flow on the rotor blade strongly depends on rotor azimuth, flow separations as well as shock waves are of high dynamic nature and therefore cause vibrations.

In low speed flight as well as descent flight, rotor noise and vibration are mainly determined by blade vortex interactions (BVI). In contrast to fixed-wing aircrafts for which tip vortices are moving downstream away from the wing, those created by helicopters remain in the vicinity of the rotor for several revolutions. This causes multiple blade vortex interactions when rotor blades

encounter previously generated tip vortices or pass them very close. Consequently, the velocity field around the blades is changing and the altered angle of attack generates unsteady airloads on the blades which originate noise and vibration.

A reduction of noise and vibration is most effective when the disturbing forces are attenuated at their origin e.g. by an individual control of the blades. A promising approach is the use of anisotropic piezoelectric strain actuators embedded in the rotor blade structure, capable of generating a direct twist deformation of the rotor blade. In comparison to approaches using flaps that generate an aerodynamic moment to deform the blade, the complexity of the actuation system is rather low. Since no moving parts are involved and there is no friction and wear. This is of special importance in a helicopter environment with high centrifugal forces. The same applies for the fact that no heavy mechanical components have to be installed inside the blade causing high loads and can also lead to a weakening of the rotor blade structure. In addition to that the active twist concept guarantees a very smooth surface of the blade whereas flaps have rough edges and therefore producing additional vortices and sources for noise and vibration.

1. STATE OF THE ART

The first active twist rotors using piezo-ceramic material to actuate the blade were presented by Chen and Chopra from the University of Maryland. From 1993 to 1996 they built and hover tested a series of 1/8th Froude scaled model rotors. The rotor blade skins incorporated piezoceramic plates using the transversal piezoelectric d_{31} -effect [1].

In 1995 a team joining researchers from Boeing, Penn State University and MIT started investigating in the field of active rotors. After proving the concept with a 1/16th Froude scale model rotor, they investigated the capability of active twist of two 1/6th Mach scale rotors (Active Material Rotor AMR). Since at this moment it was not sure whether the generation of structural twist or the twist generation via flaps is favorable, the first phase of this project included the design, manufacturing and testing of both design principles. At the beginning of the project the active twist concept was rated as the high risk approach whereas the flap design was considered to have low risk. This direct comparison by the same team of engineers developing both concepts side-by-side pointed out many advantages of the active twist concept. Actually the active twist concept turned out to be the low risk approach. Because of the encouraging results the active twist concept was applied to a modern planform and airfoil rotor blade. The active twist blades were actuated by interdigitated piezo fiber composites integrated in the spar of the rotor blade [2].

In 1999 a joint venture from NASA, Army and MIT built and tested an active twist rotor (ATR) with a structural design similar to the Boeing model rotor. This rotor was conceived for the testing in heavy gas medium, in the NASA Langley Transonic Dynamics Tunnel. This rotor is the only one which is wind tunnel tested under forward flight conditions. The twist is generated via Active Fiber Composite piezoelectric actuators embedded into the rotor blade spar. [3, 4, 5].

In 2004 Boeing investigated the possibility of scaling the results of the Mach-scaled rotor to a full scale rotor blade. The main focus of this investigation was laid on production and manufacturing approaches concerning the incorporation of the piezoelectric actuators and a robust and reliable wiring to provide the necessary power to the actuators. A 1.8m CH-47D blade section with 24 layers of active fiber composites embedded in the spar laminate was build and successfully tested. It was shown that a full scale active twist blade with a meaningful actuation

capability and acceptable natural frequencies can be built within the weight limit of a passive blade [6].

Motivated by these promising results and the potential benefits, the goal of this work was the development and test of an active twist blade incorporating improved actuation technology and alternative structural concepts to bring this technology a further step forward. At this phase the test are limited to a verification of the actuation system and the structural concepts under centrifugal loads. The intention is to develop the necessary prerequisites for a successful wind tunnel campaign with an active twist model rotor.

2. DESIGN AND MANUFACTURING OF THE ACTIVE TWIST BLADE

In the design phase of the blade, several parameter studies were carried out, resulting in an optimal orientation for the ply lay-up of the skin as well as the actuation direction [7]. This optimum considers the twist deflection that can be achieved with respect to the torsional rigidity. The optimal configuraton lead to a blade with an anisotropic skin. With regard to these findings a model rotor blade was built. The main characteristics of this blade were taken from the well known BO 105 model rotor blade. The BO-105 blade features a C-Spar made of unidirectional glass fiber, a glass fiber skin and a foam core (Figure 1). The chord length of 121mm and the radius of 2m are in agreement with the original model rotor blade, whereas the profile was changed into a symmetrical NACA 0012, which does not really change the blade from a structural point of view. Because at this point no aerodynamic investigations were planed, it was not necessary to realize an aerodynamic effective blade and the manufacturing effort was reduced by building only one mold. For the same reason the blade was not pre-twisted. The actuator orientation was chosen to be $+40^\circ$, whereas the skin was made of unidirectional glass fiber laminates with an orientation of -30° (inner skin). The area surrounding the actuators was provided with additional unidirectional glass fiber layers in a $+40^\circ$ direction in order to carry the loads of the actuators and to decrease the change in stiffness in the transition region between skin and actuators. The anisotropy of the skin allows the actuators to work in a relatively soft direction (approximately perpendicular to the fibers in the inner skin), whereas the complete blade still keeps its torsional stiffness by the shear stiffness perpendicular to the actuators.

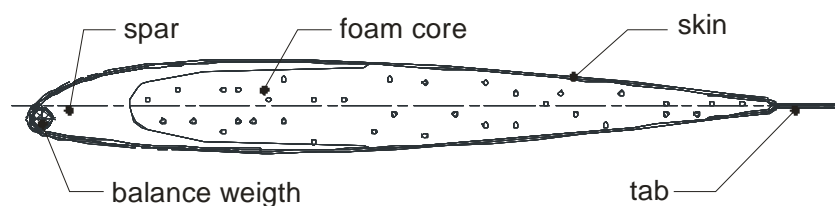


Figure 1: cross section of the original BO105 model rotor

A special focus was laid on the selection and design of the piezoelectric actuators. In all previous investigation (see chapter 1) so called Active Fiber Composite (AFC) Actuators were used [8]. In this assembly a large number of PZT-fibers with typical diameters of 100-250 μ m are aligned side by side and are usually embedded in an epoxy resin (Figure 2a). To benefit from the higher longitudinal effect (d_{33} -effect) interdigitated electrodes (IDE-Electrodes) are used. This design is realized with two interlaced comb like electrodes symmetrically arranged on each side. With high voltages applied to the electrode fingers the polarization of the PZT material is established to fit to the electrode structure. An essential drawback of this concept is the very labor intensive manufacturing process. Up to know it is primarily handwork to place the many single fibers close to another. This causes quality problems, resulting in deviations of the actuator

characteristics. Since the fibers have a circular cross-section the electrode contacts the piezoelectric material only over a small area, leading to significant dielectric losses.

An alternative manufacturing process uses cheap PZT-wafers that are cut into ribbons (Figure 2b). In this case the wafer is placed on a tacky film and cut using a wafer saw, typically used within the production of computer chips. With this automated process the ribbons are aligned exactly in parallel. In the following manufacturing steps the gaps between the ribbons are filled with resin and polyimid films with etched IDE-electrodes are glued on the top and the bottom of the assembly. Due to the rectangular cross section of the ribbons the connectivity of the electrode to the piezoelectric material is considerably improved. This design has been developed by NASA [9] and is called Macro Fiber Composite (MFC).

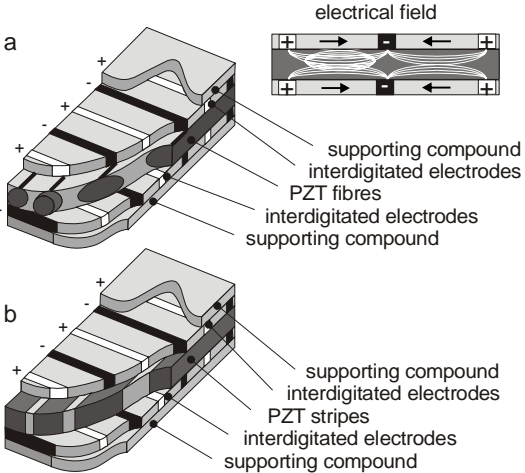


Figure 2: AFC design with fibers; b) MFC design with ribbons



Figure 3: special shaped MFC actuators; height 60,2mm; width 222mm

To provide a good coverage with active material and to realize the desired actuation direction of 40°, special shaped MFC actuators were designed for the active twist blade (Figure 3). Due to their particular electrode design these types of actuators have to be operated at relatively high voltages between -500 V and +1500 V to provide a sufficient electrical field. A total of six actuators per skin were implemented, resulting in a total active area of approx. 1600 cm².

The manufacturing process of the upper and lower blade skin started with the placement of the MFC actuators into the mould followed by the glass fiber prepreg. Accordingly the strain gauge instrumentation and the complete wiring were positioned onto the uncured prepreg. In the next step the lay-up was put in a vacuum bag and cured in an autoclave at a temperature of 120°C and a pressure of 6 bars. Because actuation and instrumentation are entirely integrated into the rotor blade skins, it was possible to keep the internal design similar to that of conventional passive blades. The spar and the foam core were machined to the desired shape using unidirectional glass fiber composite and foam blocks, respectively. Balancing weights made of tungsten rods were added into the nose of the spar using a cold setting epoxy. Finally the upper and lower skin, the spar and the foam core were bonded together with an adhesive film and cured at 120°C.



Figure 4: top view of the active twist blade

2. EXPERIMENTAL TEST SETUP

The objective of the test was to demonstrate the performance of the actuation system and the structural concept under centrifugal loads by showing that the expected twist deformation can be achieved at the nominal rotation speed and different actuation frequencies. For this purpose a test rig was installed at the DLR rotor tower in Braunschweig (Fig .5). The test rig is driven by a 30kW DC shunt-wound motor. A balancing weight is mounted on the opposite side to trim the blade. The direction of rotation is clockwise. To reduce the mechanical complexity the pitch links have been removed. Data transfer is realized by 24 slip rings and an additional telemetry system with 12 channels for strain gauge measurements (full bridge or half bridge) and 4 ICP channels for acceleration sensors. Four special designed high voltage slip rings transfer the required electrical power to the actuators in the blade. Depending of the excitation frequency the actuators were driven with up to three power amplifiers with a peak to peak voltage of $\pm 2000V$ and a maximum current of 400mA. A camera, installed in the rotor tower, allows a permanent monitoring of the experiment from the control room.

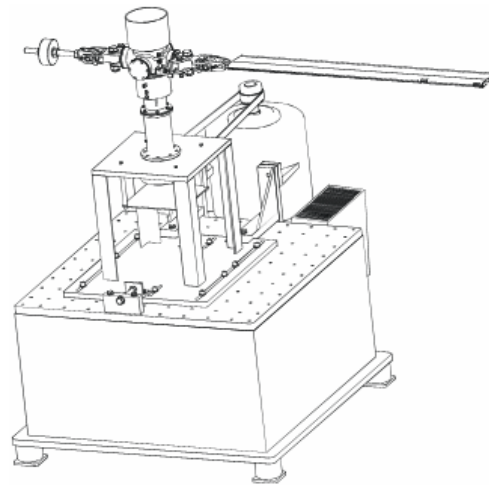


Figure 5: test rig

The Active Twist Blade was equipped with nine sets of strain gauges. Six sets were implemented for measurement of torsion (one for each actuator) and 3 for flapping. The locations of the strain gauges are shown in Figure 6. As described before the strain gauges and the necessary wiring were embedded into the blade skin during the manufacturing process. For each torsion measurement point, two strain gauges were arranged on opposite sides of the upper and lower blade shell in an angle of $\pm 45^\circ$ degree to measure the torsional deformation of the blade. The individual strain gauges were wired to a full bridge to compensate for any bending deformation of the blade, so that only torsional deformations were measured. Since it is not possible to directly measure the twist angle with strain gauges, two additional acceleration sensors were mounted at the leading and trailing edge of the blade tip respectively. As backup and to check the results of the strain gauge and acceleration sensor measurements, a supplementary optical measurement system was installed. The system consists of two LED's attached at the leading- and trailing edge of the rotor blade tip and a stationary high speed camera system. By properly triggering the camera the twist movement of the blade can be visualized by the two light dots of the LED's. In comparison to a system that needs a powerful stroboscope light, capable of sufficiently illuminate the blade tip, this solution is much cheaper and also facilitates the analysis of the blade tip motion. Because the LED's appear as clearly distinguishable points, standard image processing tools can be used to automatically determine the twist angle.

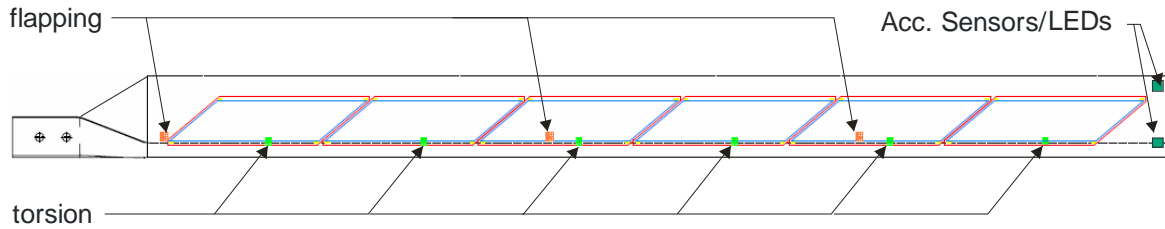


Figure 6: sensor positions

3. EXPERIMENTAL RESULTS

Before the centrifugal test was conducted, the static properties of the Active Twist Blade were measured within a simple lab test configuration. Table 1 compares some of these results with the results of a finite element simulation and the properties of the BO-105 reference rotor. There is a reasonable good correlation between the measured and simulated stiffness parameters and the active performance. In comparison with the reference rotor all parameters of the Active Twist Blade stay within the tolerated limits.

| Parameter | Experiment | Simulation | Ref. (BO 105) |
|---|---------------------|---------------------|---------------------|
| Flap bending stiffness | 196 Nm ² | 207 Nm ² | 250 Nm ² |
| Torsional stiffness | 194 Nm ² | 189 Nm ² | 160 Nm ² |
| Twist rate ($\Delta U = -500..+1500$) | 2.87 °/m | 2.7 °/m | - |

Table 1: comparison of measured and calculated data of the AT1-blade

For the centrifugal tests a comprehensive test matrix was derived starting with the measurement of the static peak to peak twist displacement with increasing rotation speed starting from 400 RPM up to the nominal rotation speed of 1043 RPM (109 rad/s; 17,35 Hz) in steps of 100 RPM. All measurements were made using the optical measurement system. The actuators were driven within a voltage range of -500V to +1300V with a quasi static excitation of 0.15 Hz. Though a maximum of +1500V is allowed for the MFC actuators the actuation voltage was reduced to 1300V to avoid any electrical overload. In Figure 7 the result of the measurement with reduced actuation voltage are plotted as well as the linear interpolated twist deflection with a maximum voltage of 2000 V_{pp} (-500V...+1500V).

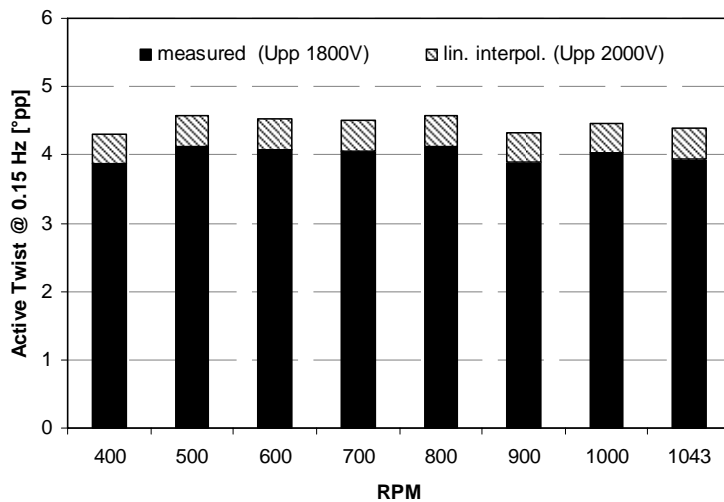


Figure 7: quasi static excitation of the blade at different rotation speeds

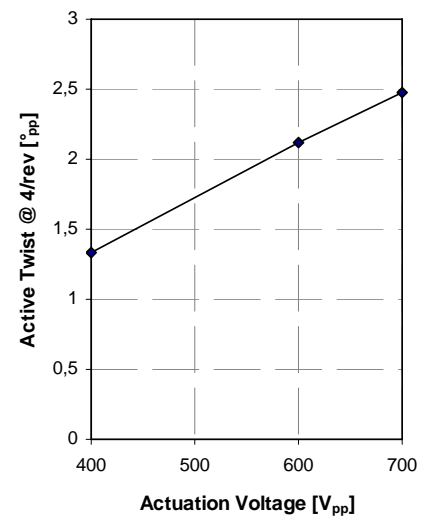


Figure 8: linear correlation between actuation voltage and twist deflection

For all rotation speeds the tip twist is in the order of 4° peak to peak with a deviation of $\pm 0.1^\circ$, which is due to the measurement accuracy. This measurement confirms, that the actuation system is capable of generating sufficient twist under centrifugal loads and that there is no performance decrease in comparison to the no rotating case.

The validity of the assumption of a linear correlation between twist deflection and actuation voltage is supported with the measurements plotted in Figure 8. For different voltages the twist was measured at a rotation speed of 1043 RPM and an excitation frequency of 69.5 Hz. Due to the material inherent nonlinearity of the piezoelectric actuators this assumption can only be an approximation but is reasonable for this case.

The next test comprised a measurement of the tip twist at different excitation frequencies from 2/rev (34,8 Hz) to 6/rev (104,3 Hz). All measurements were done at the nominal rotation speed of 1043 RPM using the optical measurement system. The results are shown in Figure 9. The actuators were again only driven with a limited voltage of $1800 V_{pp}$. At a frequency of 2/rev the tip twist is equal to the quasi static twist. Because of resonance effects in the vicinity of the first torsional eigenfrequency the amplitude at 3/rev and 4/rev is even higher ($>6^\circ$). A look at the rotor diagram (Figure 10) for the first and second torsional eigenmodes explains why the measurement at 4/rev was only done with a very reduced voltage of $700 V_{pp}$. Unfortunately the first torsional eigenmode is very close to 4/rev. Therefore the voltage was reduced to avoid any catastrophic resonance effects.

For the determination of the torsional eigenfrequencies only the upper and lower MFC actuators next to the blade root were excited with a low voltage sinusoidal sweep ranging from 0 to 400 Hz. Here the signals were acquired from strain gauges and acceleration sensors.

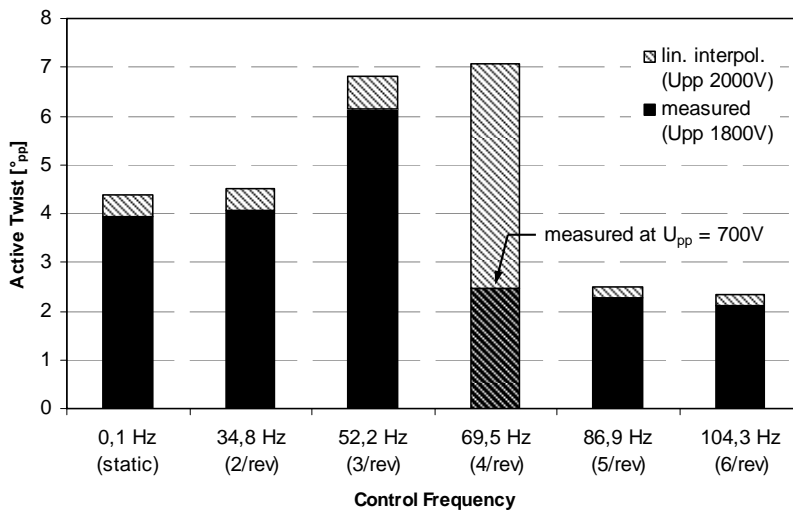


Figure 9: dynamic excitation at different control frequencies at 1043 RPM

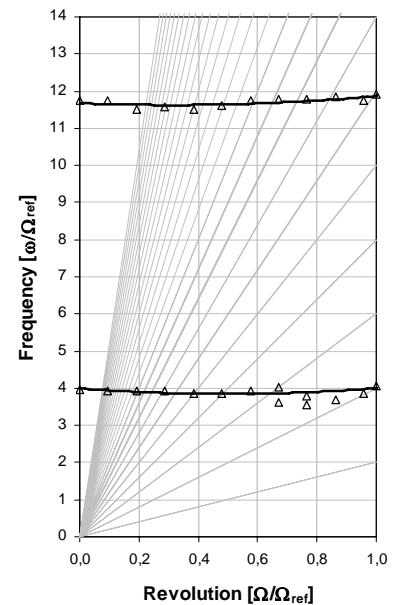


Figure 10: rotor diagram for the 1st and 2nd torsional eigenmode

The reduced twist performance at 5/rev and 6/rev is mainly caused by the influence of second mode shape. In this case there is no steady increase of the twist deflection along the span width, and the actuators on both sides of the vibration node are operating counterproductive. To compensate for this problem an individual control of the MFC actuators along the span width

was realized and investigated. In Figure 11 the results of a measurement at 1043 RPM, at an excitation frequency of 6/rev using a different number of activated actuator segments are plotted. The maximum twist deflection is achieved when only actuator segment three to six are activated. This indicates that there is a vibration node between segment three and two what is confirmed by strain gauge measurements. Ongoing activities are dealing with the development of optimized control laws to improve the twist deflection of the blade above the first torsional eigenfrequency.

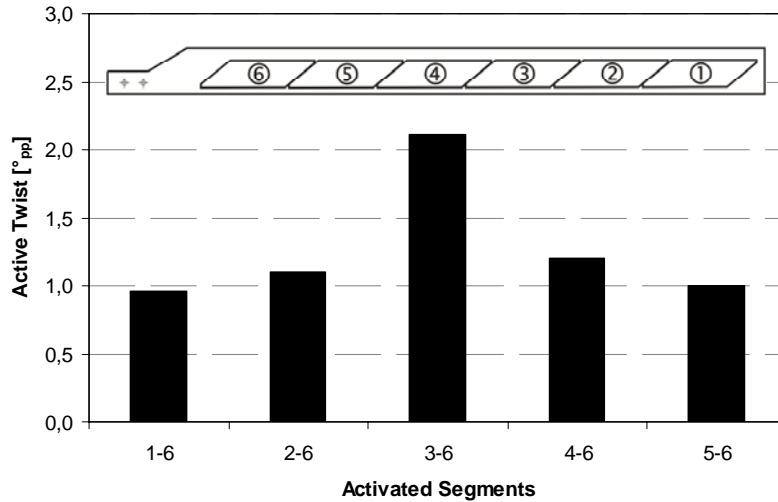


Figure 11: Influence of a segmented excitation of the blade at 6/rev (104,3 Hz) and 1043 RPM

4. ROTOR SIMULATION

In addition to the structural design and testing of the active twist blade also an aeromechanical rotor simulation was run to evaluate the potential of the blade concerning noise and vibration reduction in forward flight. For an analysis of the rotor behavior regarding to noise, a descent flight was chosen as a typical flight condition where very intensive BVI noise is radiated from the rotor. As described above, intensive vibrations are dominating in high speed forward flight. Thus, a high speed forward flight was chosen to examine the rotor characteristics concerning vibration. Table 2 summarizes the definitions for the noise and vibration flight case.

| Parameter | Descent Flight | High Speed Forward Flight |
|---------------------|----------------|---------------------------|
| μ | 0.151 | 0.319 |
| α_{sh} / deg | 4.4 | -8.8 |
| C_T/σ | 0.056 | 0.067 |
| M_{tip} | 0.64 | 0.63 |

Table 2: Definition of flight cases for the analysis of the noise and vibration rotor characteristics

Rotor simulations were performed employing the aeromechanical simulation code S4. Within S4, aerodynamics are considered as unsteady. For the computation of the induced velocities, a prescribed wake model is included [10]. The wake model is taking into account additional deformation of the rotor wake due to higher harmonic lift components [11] where double vortex systems, which arise when the blade tip generates download, are implemented. Blade dynamics are represented by the Eigenmodes of the blade in flapping, lagging and torsion.

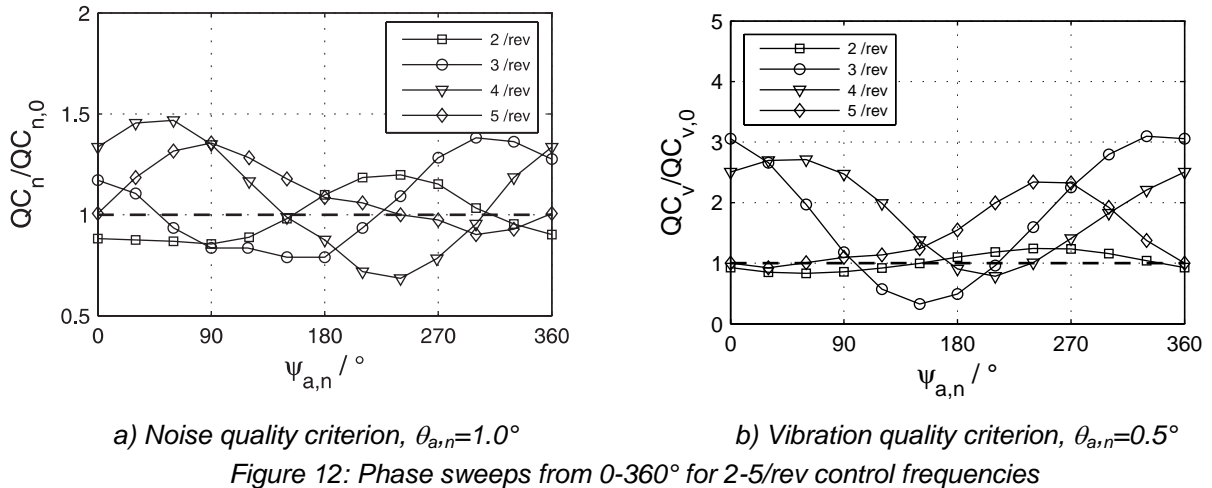
| Parameter | Definition |
|---------------|--------------|
| airfoil | NACA23012 |
| c | 0.121 m |
| N_b | 4 |
| R | 2 m |
| scale factor | 2.5 |
| θ_{tw} | -8° |
| σ | 0.077 |
| Ω | 109.27 rad/s |

Table 3: Rotor data of the AT2

The model rotor is based on a BO105 rotor blade with the rotor specifications as given in Table 3. To be as close to reality as possible, the rotor data defined from the structural design process have been replaced by experimental data where available. Thus, the model rotor is specified from a semi-empirical data set. The active twist area extends from a radial position of $0.275R$ up to $0.96R$. The maximum control amplitude at the blade tip is used as input within the simulation program. As a simplification, the control amplitude is prescribed to rise linear from the initial radius up to the outer radial position of the active blade area independently of the control frequency.

4.1 Noise and Vibration Benefits

To obtain a general idea of the rotor behavior towards different active twist control inputs, frequency sweeps as well as phase sweeps were performed. Based on a cosine signal, control frequencies of 2-5 integer multiples of the rotor rotational frequency (1/rev) were applied, varying the control phase by increments of 30° from $\Psi_{a,n}=0-360^\circ$ (Figure 12).



For the investigation of the noise characteristics, a control amplitude of $\theta_{a,n}=1^\circ$ was applied. From an analysis of the high-frequency components of the lift coefficients, a noise quality criterion has been calculated by S4. QC_n is computed as the sum of the $\partial C_n M^2 / \partial \Psi$ gradients in rotor areas where parallel BVI occurs since parallel BVI extends over a large radial area of the blade and thus originates intensive BVI noise. Those BVI areas are located between $\Psi=20^\circ-100^\circ$ at the advancing side and $\Psi=270^\circ-330^\circ$ at the retreating side. The noise criterion is

weighted azimuthally taking into account the degree of BVI parallelism. Additionally, QC_n is weighted radially to consider the influence of the increasing Mach number going up to the blade tip. To obtain an overall criterion, the noise criteria for advancing and retreating side are accumulated.

Figure 12a illustrates the noise quality criterion QC_n referred to the quality criterion of the baseline case without active control $QC_{n,0}$. A 3/rev and 4/rev control frequency seem to be most efficient regarding to noise reductions. Minimum quality criteria are identified for control phases of $\psi_{a,3}=150^\circ/180^\circ$ respectively $\psi_{a,4}=240^\circ$. It is noteworthy, that for all of the applied control frequencies, control phases with reduced QC_n compared to the baseline case could be detected.

For a study of the vibration behaviour of the rotor, a rather low control amplitude of $\theta_{a,n}=0.5^\circ$ has been introduced for taking into account the high sensitivity of rotor vibration towards active control. Rotor vibration is evaluated via the quality criterion QC_v which is computed by S4 (analogue to the calculation of a quality criterion for noise). The criterion is determined from the 4/rev force and moment components in the non-rotating frame since these components represent the source for vibration excitation of the helicopter airframe (1).

$$QC_v = \sqrt{\frac{F_{x,4/rev}^2 + F_{y,4/rev}^2 + F_{z,4/rev}^2}{N} + \frac{M_{x,4/rev}^2 + M_{y,4/rev}^2}{Nm}} \quad (1)$$

In high speed forward flight, control frequencies of 2-4/rev affect the vibration criteria such that for several control phases, the criteria can be reduced below the baseline value (Figure 12b). The minimum noise criterion can be found for a 3/rev control with a control phase of $\psi_{a,3}=150^\circ$. Further improvements in noise and vibration reduction are expected from an operation of optimized control laws.

Based on Figure 13, the physical background of the impact of active control on rotor noise can be discussed. The illustration shows the high-pass filtered lift distribution over the rotor disk without and with an active twist control ($\theta_{a,3}=3.0^\circ$). Since blade vortex interactions are events of high-frequency and alter the pressure and lift distribution on the blade, strong fluctuations of the normal force coefficient $C_n M^2$ indicate the appearance of BVI.

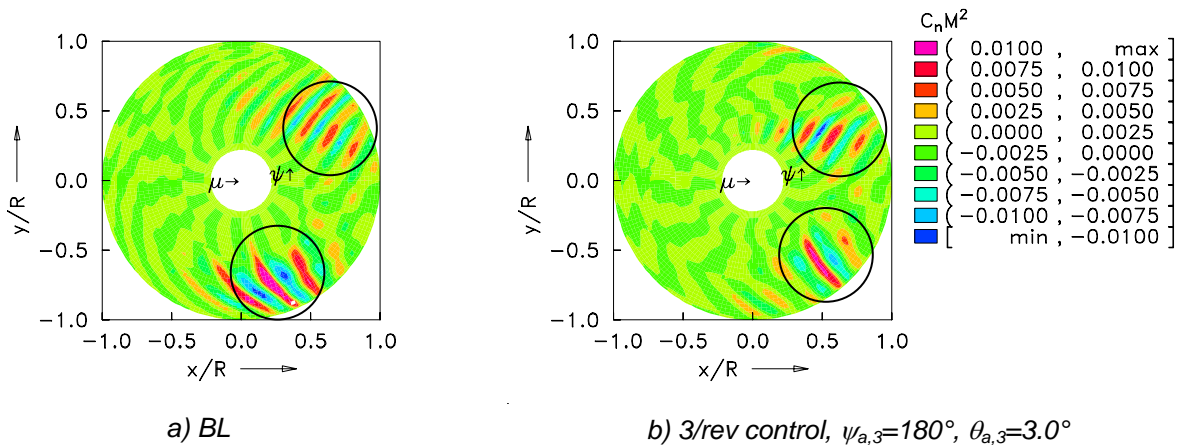


Figure 13: 12/rev high-pass-filtered $C_n M^2$; circles indicate locations of BVI

As explained before, in descent flight noise mainly is emerged from those rotor areas where parallel BVI takes place. For the baseline case without active control, large areas of blade parallel BVI can

be identified in Figure 13a for both, advancing and retreating side. By introducing an active twist control, the number and extension of parallel BVI areas is decreased at both sides of the rotor disk (Figure 13b). It can be seen that for the advancing side, BVI areas are moved more inboard. Because of the lower Mach number at inner radial positions, the generated BVI is less intensive.

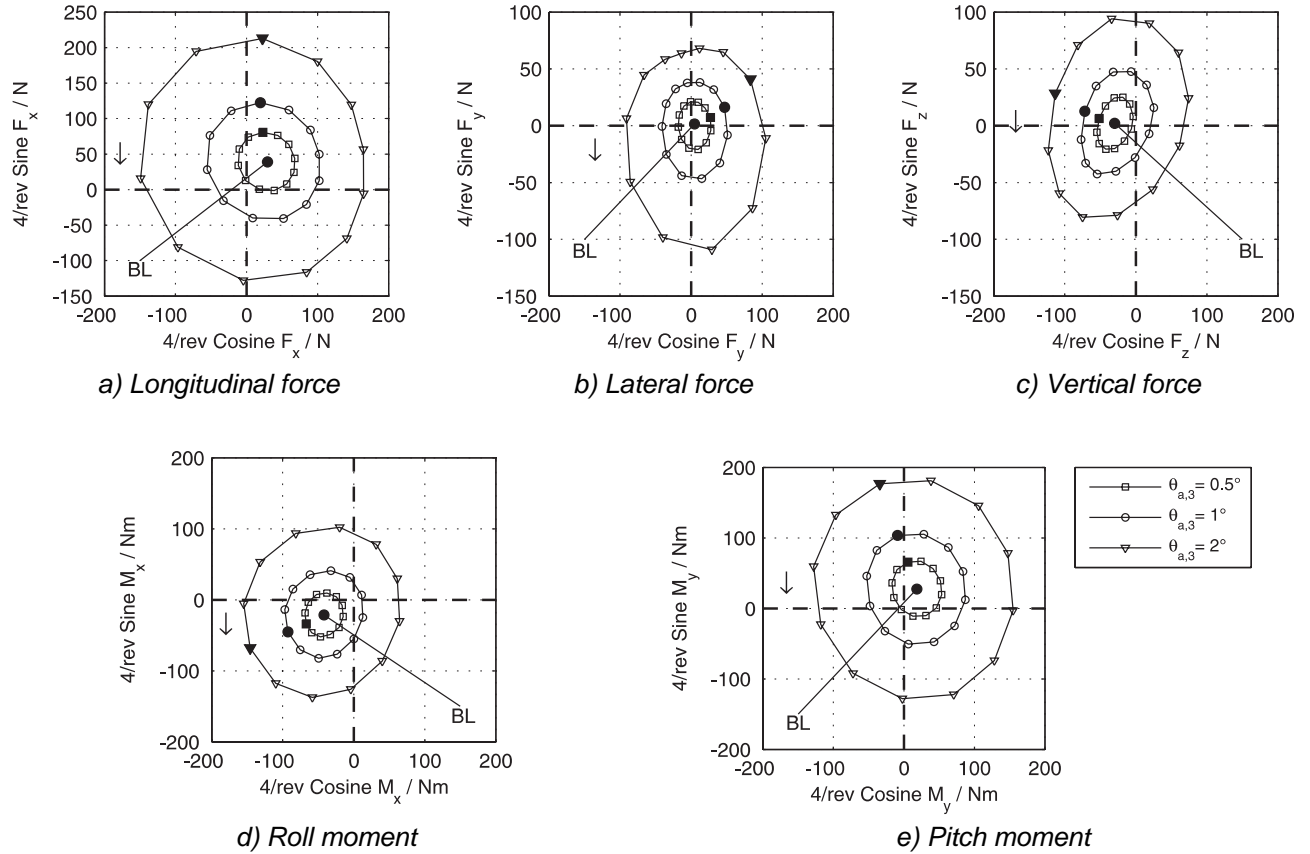


Figure 14: Force and moment response in the non-rotating frame for a 3/rev control input

A more detailed analysis of the impact of different control amplitudes, phases and frequencies on the vibration characteristics of the rotor is given in Figure 14. Here, the cosine and sine response of the 4/rev force and moment components in the non-rotating system from which the vibration quality criterion QC_v is derived, are plotted. The responses are shown for a 3/rev control frequency that provided best results in vibration reduction for the phase sweeps shown in Figure 12b. Control amplitudes of $\theta_{a,3}=0.5-2.0^\circ$ are considered for this analysis. The baseline 4/rev forces and moments are illustrated by filled circles and marked as ‘BL’. Filled symbols define the $\psi_{a,3}=0^\circ$ control phase with the direction of increasing phase denoted by an arrow. For all of the 4/rev force and moment components, beneficial control authority is gained. Already low amplitudes between approximately $\theta_{a,3}=0.5-1.0^\circ$ offer the opportunity to eliminate the 4/rev components. It is noteworthy, that for the lateral 4/rev force F_y hardly a reduction of the component is required. The sine as well as the cosine response of F_y are located near to the point of origin (Figure 14b) which means that the force component already is close to zero for the baseline case. Optimum control phases of approximately $\psi_{a,3}=120^\circ$ are in good agreement between the longitudinal 4/rev force F_x and the roll moment M_y . In contrast, for the vertical 4/rev force F_z as well as the pitch moment M_x best results are obtained employing a control phase of approximately $\psi_{a,3}=180^\circ$. Additionally, the influence of further increased control amplitudes up to $\theta_{a,3}=2.0^\circ$ is demonstrated. It can be seen that improper control amplitudes generate more vibration than the baseline case itself.

REFERENCES

- [1] Chopra, I., "Status of Application of Smart Structures Technology to Rotorcraft Systems," Journal of the American Helicopter Society, Vol. 45, No. 4, 2000, pp. 228–252
- [2] Derham, R., Weems, D. B., Mathew, M. B., & Bussom, R. C. 2001, "The design evolution of an active materials rotor", American Helicopter Society.
- [3] SangJoon Shin, Carlos E. Cesnik, Steven R. Hall, "Closed-Loop Control Test of the NASA/ARMY/MIT Active Twist Rotor for Vibration Reduction", 59th AHS Annual Forum 2003, Phoenix, Arizona, USA, 6.-8. May 2003
- [4] Wilbur, M. L., Yeager, W. T., Wilkie, W. K., Cesnik, C. E. S., & Shin, S., "Hover Testing of the NASA/ARMY/MIT Active Twist Rotor Prototype blade", American Helicopter Society, 2000
- [5] Wilbur, M. L., Mirick, P. H., Yeager, W. T., Langston, C. L., Cesnik, C. E. S., & Shin, S., "Vibratory Loads Reduction Testing of the NASA/ARMY/MIT Active Twist Rotor", American Helicopter Society, Washington, DC, 2001
- [6] Douglas B. Weems, David M. Anderson, Mathew B. Mathew, Richard C. Bussom, "A Large-Scale Active-Twist Rotor", 60th AHS Annual Forum, Baltimore, MD, USA, 7.-10. June 2004
- [7] Riemenschneider, J., Keye, S., Wierach, P., & Mercier des Rochettes, H., "Overview of the Common DLR/ONERA Project Active Twist Blade", 30th European Rotorcraft Forum, Marseille, 2004
- [8] Bent, A. A., Hagood, N.W., and Rodgers, J.P., „Anisotropic Actuation with Piezoelectric Fiber Composites“, Journal of Intelligent Materials Systems and Structures, Vol. 6, May 1995
- [9] Wilkie, W., High, J., Mirick, P., Fos, R., Little, B., Bryant, R., Hellbaum, R., Jalink, A., "Low Cost Piezocomposite Actuator for Structural Control Applications“, Proceedings SPIE's 7th International Symposium on Structures and Materials, Newport Beach, California, March 5-9, 2000
- [10] T. S. Beddoes, „A Wake Model for High Resolution Airloads“, Proceedings of the International Conference on Helicopter Basic Research, Army Research Office, Research Triangle Park, NC, USA, 1985
- [11] B. G. van der Wall, „Simulation of HHC on Helicopter Rotor BVI Noise Emission using a Prescribed Wake Method“, 26th European Rotorcraft Forum, The Hague, Netherlands, 2000

NOMENCLATURE

| Symbols | Variable | Unit |
|----------------|---|-------------------|
| a_∞ | speed of sound | m/s |
| c | blade chord | m |
| C_n | normal force coefficient | - |
| C_T | thrust coefficient, $C_T=T/(\rho\pi R^2(\Omega R)^2)$ | - |
| F | force | N |
| M | moment | Nm |
| M_{tip} | Mach number at the blade tip, $M_{tip}=\Omega R/a_\infty$ | - |
| N_b | number of blades | - |
| QC_v | vibration quality criterion | - |
| QC_n | noise quality criterion | - |
| R | blade radius | m |
| T | thrust | N |
| V_∞ | flight speed | m/s |
| x, y, z | coordinates | m |
| α_s | angle of attack of the rotor shaft | deg |
| θ_{tw} | blade twist angle | deg |
| $\theta_{a,n}$ | control amplitude of active twist | deg |
| μ | advance ratio, $\mu=V_\infty \cos\alpha_s/(\Omega R)$ | - |
| ρ | air density | kg/m ³ |
| σ | rotor solidity, $\sigma=N_b c/(\pi R)$ | - |
| Ω | rotor rotational speed | rad/s |
| $\Psi_{a,n}$ | control phase referred to the control input | deg |
| Indices | | |
| a | due to active control | |
| n | n-th harmonic | |
| s | rotor shaft | |
| tip | blade tip | |
| tw | twist | |
| 0 | baseline, without active control | |
| ∞ | properties of undisturbed flow | |